Functional connectivity alterations in traumatic brain injury patients with late seizures

Marianna La Rocca [a,b,e,*], Giuseppe Barisano [b], Rachael Garner [b], Sebastian F. Ruf [c], Nicola Amoroso [d,e], Martin Monti [f], Paul Vespa [g], Roberto Bellotti [a,e], Deniz Erdoğmuş [c], Arthur W. Toga [b], Dominique Duncan [b], for the EpiBioS4Rx Study Group

[a] Dipartimento Interateneo di Fisica M. Merlin, Universitá degli Studi di Bari A. Moro, Bari, Italy
[b] Laboratory of Neuro Imaging, USC Stevens Neuroimaging and Informatics Institute, Keck School of Medicine of USC, University of Southern California, Los Angeles, CA, USA
[c] Cognitive Systems Laboratory, ECE Department, Northeastern University, Boston, MA, USA
[d] Dipartimento di Farmacia - Scienze del Farmaco, Università degli studi di Bari A. Moro, Bari, Italy
[e] Istituto Nazionale di Fisica Nucleare, Sezione di Bari, Italy
[f] Department of Psychology, University of California, Los Angeles, Los Angeles, CA, USA
[g] David Geffen School of Medicine, University of California, Los Angeles, Los Angeles, CA, USA

ARTICLE INFO

ABSTRACT

PTE is a neurological disorder characterized by recurrent and spontaneous epileptic seizures. PTE is a major public health problem occurring in 2–50% of TBI patients. Identifying PTE biomarkers is crucial for the development of effective treatments. Functional neuroimaging studies in patients with epilepsy and in epileptic rodents have observed that abnormal functional brain activity plays a role in the development of epilepsy. Network representations of complex systems ease quantitative analysis of heterogeneous interactions within a unified mathematical framework. In this work, graph theory was used to study resting state functional magnetic resonance imaging (rs-fMRI) and reveal functional connectivity abnormalities that are associated with seizure development in traumatic brain injury (TBI) patients. We examined rs-fMRI of 75 TBI patients from Epilepsy Bioinformatics Study for Antiepileptogenic Therapy (EpiBioS4Rx) which aims to identify validated Post-traumatic epilepsy (PTE) biomarkers and antiepileptogenic therapies using multimodal and longitudinal data acquired from 14 international sites. The dataset includes 28 subjects who had at least one late seizure after TBI and 47 subjects who had no seizures within 2 years post-injury. Each subject's neural functional network was investigated by computing the correlation between the low frequency time series of 116 regions of interest (ROIs). Each subject's functional organization was represented as a network consisting of nodes, brain regions, and edges that show the relationship between the nodes. Then, several graph measures concerning the integration and the segregation of the functional brain networks were extracted in order to highlight changes in functional connectivity between the two TBI groups. Results showed that the late seizure-affected group had a compromised balance between integration and segregation and presents functional networks that are hyperconnected, hyperintegrated but at the same time hyposegregated compared with seizure-free patients. Moreover, TBI subjects who developed late seizures had more low betweenness hubs.

1. Introduction

Traumatic brain injury (TBI) is a leading cause of death and disability in the world, accounting for 2.5 million emergency department visits annually in the United States. TBI survivors often experience secondary problems that result in serious and persistent sequelae and psychosocial difficulties. Recurrent and unprovoked seizures are among the most recognized complications of TBI (Lucke-Wold et al., 2015; Sharma et al., 2021). The incidence of epilepsy after TBI is up to 50% depending on the TBI severity and the follow-up duration. Post-traumatic epilepsy (PTE) refers to recurrent and unprovoked late seizures (occurring more than seven days after TBI) (Cavazos and Verellen, 2010). Immediate

* Corresponding author at: Dipartimento Interateneo di Fisica M. Merlin, Universitá degli Studi di Bari A. Moro, Bari, Italy.
E-mail address: marianna.larocca@uniba.it (M. La Rocca).

(occurring less than 24 h after TBI) and early seizures (occurring between 24 h and seven days after injury) are considered to be the result of acute TBI and do not constitute an epilepsy diagnosis. Since PTE is highly variable and time from TBI to epilepsy onset may span several years, preventing epileptogenesis and improving pre-clinical models that adequately represent posttraumatic epilepsy is rather challenging. In fact, effective interventions to prevent epileptogenesis are lacking and little is known about PTE trajectory from the early stages post-injury. The Epilepsy Bioinformatics Study for Antiepileptogenic Therapy (EpiBioS4Rx) was designed to identify a combination of biomarkers that will reliably predict epileptogenesis following TBI in both a rodent model and humans and identify specific antiepileptogenic treatments to be used in future clinical trials (Garner et al., 2019; Peterson et al., 2019; La Rocca et al., 2020).

Blood oxygenation level dependent (BOLD) functional magnetic resonance imaging (fMRI) detects changes in blood oxygenation that are related to neuronal activity. It is a neuroimaging technique that allows for visualization of whole-brain activity and can be used to identify and investigate functional brain networks. During rest, basic neuronal activity is believed to induce low frequency fluctuations in the BOLD signal that can be detected by performing resting state fMRI (rs-fMRI). A technique called functional connectivity analysis allows one to compute the correlation between the low frequency fluctuations and identify brain regions that are functionally connected. The functional organization of the brain can be investigated using different analytic methods, including seed-based correlation, independent component analysis (ICA) and graph theory (Smitha et al., 2017). In graph theory, the brain is represented as a network consisting of nodes, usually brain regions, and edges that show the relationship between the nodes. Several graph theoretical measures can be calculated to describe and quantify the network (Bellantuono et al., 2021; Rasero et al., 2017). Changes in these measures, and thus in functional connectivity, have been found in various neurological disorders, including Alzheimer's disease, schizophrenia, attention-deficit hyperactivity disorder, traumatic brain injury and epilepsy (Wang et al., 2010; Rubinov and Sporns, 2010).

Studies combining rs-fMRI with graph theory in patients with epilepsy have shown abnormalities in the topological organization of the brain. Most studies found a lower segregation and increased integration (Liao et al., 2010; Song et al., 2015; Mazrooyisebdani et al., 2020). Vlooswijk et al. (2011) also found decreased segregation, but accompanied by decreased integration. Whereas, Peterson et al. (2019), Wang et al. (2014) found both a higher integration and segregation, even though the latter states that this can be due to medications or a brain mechanism to avoid seizure spread that is specific for focal forms of epilepsy.

In this work, we characterized, for the first time, the functional brain network organization of TBI subjects and investigated how this functional organization changes in TBI subjects who develop epilepsy. Various graph theory metrics concerning network integration, segregation and centrality were used. Usually, functional connectivity studies are based on network metrics computed from binary brain networks leaving out the network weights. Even though unweighted networks have the advantage of easier interpretation, they can overlook the diversity of temporal correlations among different brain regions (Wang et al., 2019; Ma et al., 2018). Therefore, to obtain a comprehensive description of the functional brain networks associated with TBI, we performed both unweighted and weighted network analyses. It is well-known that the human brain optimizes the balance between the cost of maintaining many connections and the efficiency of transmitting information through a small-world architecture. Small-world topology occurs when there are many short range connections between related areas and relatively few long range connections between less related areas (Watts and Strogatz, 1998). Several studies have observed that this optimal organization can be disrupted by aging as well as brain diseases (Brier et al., 2014; Achard and Bullmore, 2007). While small-world behavior has been investigated in TBI patients and in subjects with

temporal lobe epilepsy and other forms of epilepsy, how small-world properties of the brain are changed by seizure development in TBI patients has not yet been investigated (Pandit et al., 2013; Yang et al., 2018). In this regard, we deepened also this aspect of the brain small-world topology. Another important aspect of human brain networks are the network hubs, which are nodes with a large number of connections. It has been shown that these strategical nodes are particularly vulnerable to targeted attacks that are generally associated with the progression of neurodegenerative conditions (Tijms et al., 2013). Therefore, another crucial aim of this study was to identify the hubs which characterize the functional networks of TBI patients and how these nodes can be affected by seizure development. In summary, the main goals of this work are three: (i) the study of the functional connectivity in TBI patients to highlight alterations related to late seizure development, (ii) the characterization of the functional brain network organization in TBI patients who developed at least one late seizure and (iii) the characterization of the ROIs that are functionally strategical in TBI patients who developed at least one late seizure.

2. Materials and methods

2.1. Dataset

This is a prospective multicenter observational biomarker study of moderate-severe TBI patients and was approved by the UCLA Institutional Review Board and the local review boards at each EpiBioS4Rx Study Group institution. All patients have consented for data to be deidentified and then analyzed. In this study, we used 75 rs-fMRI scans of TBI subjects enrolled in EpiBioS4Rx according to specific inclusion and exclusion criteria available online.[1] Of these subjects, 28 experienced at least one late seizure within 24 months of their TBI and 47 did not experience any seizures. Both groups include acute, sub-acute and chronic TBI and the distributions of the MRI post-injury days (see Fig. S1 in the Supplementary Material) are not different for the two groups at a 1% significance level using the Wilcoxon rank-sum statistic test. Demographic and clinical information for the two groups are reported in Table 1. In addition a breakdown of the late seizure onset period for each patient is reported in the Supplementary Material (Fig. S2).

2.2. Imaging acquisition

Images were from: Siemens 3T Skyra at Massachusetts General Hospital; Philips Healthcare Ingenia 3T at Phoenix Children's Hospital; GE Healthcare Signa HDxt 3T at University of California, Davis; Siemens 3T TrioTim at University of California, Los Angeles; GE Healthcare SIGNA Architect 3T at University of Cincinnati; Siemens Aera 1.5T at

Table 1
Sample size, gender, and Glasgow Coma Score (GCS) at emergency department arrival are reported for each clinical class. Age and GCS were provided in terms of mean and standard deviation. No statistically significant differences between the two classes were found with respect to age, GCS score, and gender. Statistical evaluations were performed with a Wilcoxon rank-sum statistic test except for gender, for which a Chi-square test was used.

Clinical status	Sample size	Age	Female/Male	GCS score
Seizure-free patients	47	43.77 ± 20.75	11/36	8.26 ± 4.43
Patients with late seizure	28	38.21 ± 18.24	6/22	7.07 ± 3.57

---

[1] https://sites.google.com/g.ucla.edu/epibios4rxmobilewebsite/inclusion exclusion-criteria.

University of Miami; Siemens 3T Verio at Yale University; and Siemens 3T Skyra at Alfred Hospital. Imaging was performed within 36 days of TBI using a standardized protocol. MRI sequences acquired included resting state blood oxygen level dependent imaging (rs-BOLD), 3D T1-weighted magnetization prepared rapid gradient-echo (MPRAGE) and 3D T2-weighted fluid attenuated inversion recovery (FLAIR). MRI acquisition parameters were optimized across sites and scanner types (1.5 and 3T) to reduce inter-scanner variability. Additional information on the recommended EpiBioS4Rx protocol used to acquire each MRI sequence is reported in Table 2.

2.3. Lesion segmentation

To incorporate lesion information in the rs-fMRI preprocessing pipeline and relate functional connectivity and lesion location, a 3D lesion mask was generated for each patient that included parenchymal contusions and brain edema. The masks were obtained via manual segmentation using ITK-SNAP (Yushkevich et al., 2006) from 3D T2-weighted FLAIR scans acquired within 36 days of TBI. Additional details on how brain contusions and edema were defined and validated are reported in La Rocca et al. (2021). Once validated, lesion masks were affinely registered to the Montreal Neurological Institute (MNI) 152 template with the Linear Registration Tool (FLIRT) of the Oxford FMRIB Software Library (FSL) for subsequent use in the rs-fMRI preprocessing pipelines (Jenkinson et al., 2012).

2.4. Preprocessing

rs-fMRI and structural MRI (sMRI) images were preprocessed using the CONN functional connectivity toolbox v18a (Whitfield-Gabrieli and Nieto-Castanon, 2012)[2]: an open source software based on SPM and MATLAB for data analysis. The CONN default pipeline was used to perform preprocessing steps on the functional and structural images as shown in Fig. 1.

First, fMRI realignment, that includes subject motion estimation and correction, was performed. Secondly, fMRIs were centered, slice time-corrected and motion artifact outliers were detected. The artifact rejection tool (ART) was used to identify outliers based on the first-order derivatives (scan to scan changes) of the associated global signal and subject movement parameters. Subject volumes were detected as outliers if satisfied at least one of the following thresholds: normalized

global BOLD signal $z \geqslant 3.0$ or $\geqslant$ 95th percentile, subject composite motion $\geqslant 0.5$ mm. As an example, the outlier identification for one subject is shown in the Supplementary Material (Fig. S3).

All sMRIs were centered and segmented into cerebrospinal fluid (CSF), gray matter (GM) and white matter (WM), and spatially normalized to the MNI152 template. Finally, fMRIs were also normalized to the MNI152, segmented into CSF, GM, and WM, and spatially smoothed to reduce noise using a 4 mm FWHM Gaussian kernel. For denoising, outliers along with CSF and white matter principal components were used as nuisance covariates in accordance with the anatomical component-based noise correction method (aCompCor) (Muschelli et al., 2014). After denoising, we isolated low-frequency fluctuations with a low-pass temporal filter (0.009–0.09 Hz).
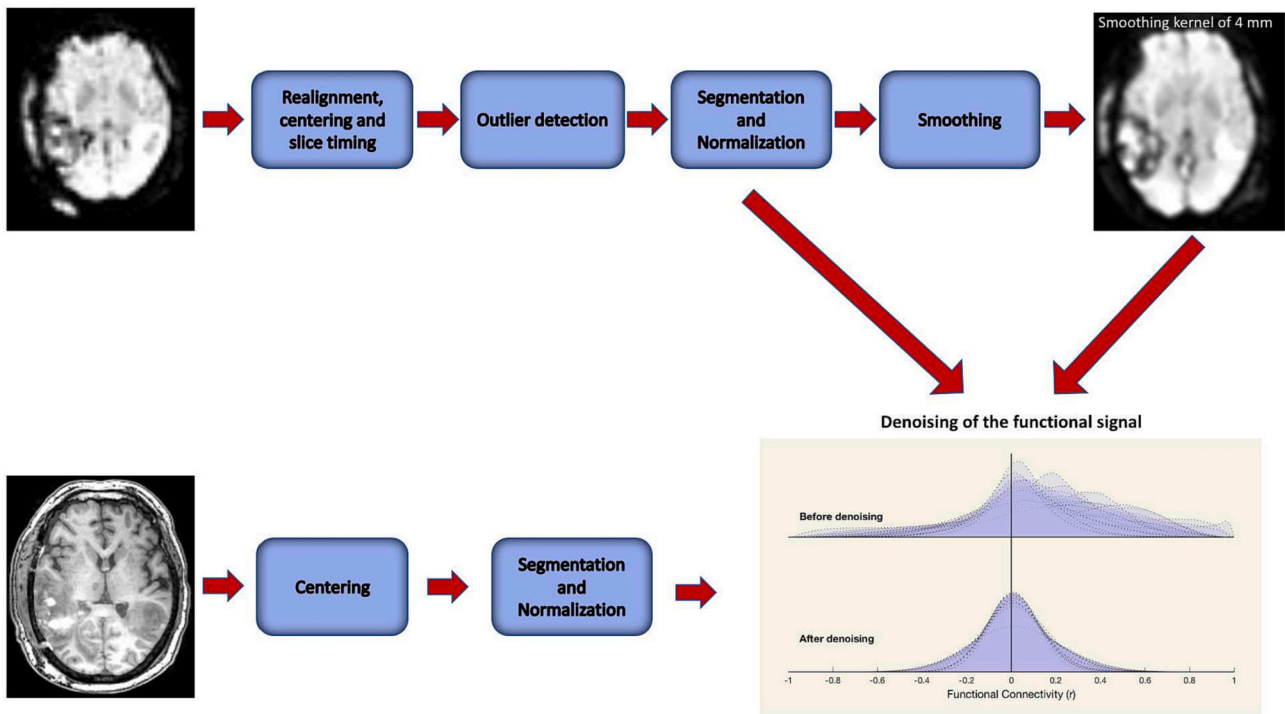
To improve tissue segmentation and noise regression, lesion information was incorporated in the segmentation step using the lesion mask (parenchymal contusions plus edema) relative to each TBI subject to obtain a modified Tissue Probability Map (TPM). The TPM normally provides a prior probability of a given voxel belonging to one of 6 tissue classes; GM, WM, CSF, skull, soft tissue, and other (Ashburner, 2009). For this pipeline the default TPM was augmented for each subject with a 7th tissue class which corresponds to the MNI lesion mask for that subject, thereby setting the prior probability of the existence of GM, WM, or CSF in the lesion areas to 0.

2.5. Graph-based network analysis

The mean BOLD signal time course was then extracted from 116 ROIs defined by the automated anatomical labeling (AAL) atlas (Tzourio-Mazoyer et al., 2002). The time series of voxels within each region was averaged and the resulting signal was used as the representative signal for that ROI. For each subject, AAL regions were employed to define the nodes of the functional brain network and Fisher z-transformed Pearson's correlation coefficients of signals of all pairs of AAL regions were computed to define the edges of the functional brain network. Therefore, we obtained an undirected weighted graph for each subject. Then, we computed the mean network for two clinical groups: seizure-free TBI patients and TBI patients who experienced at least 1 late seizure.

For each group, only positive correlations were studied because of the controversial interpretation of negative correlations in the field of brain functional connectivity. A number of studies consider negative correlations a consequence of functional signal regression. Other studies state that negative correlations can give important information about brain neuro-physiology. However they are generally fewer and less reliable than positive correlations, and their neurophysiological basis is still unclear (Schwarz and McGonigle, 2011; Fox et al., 2005; Geerligs and Henson, 2016). For each mean network, several graph theory network metrics were investigated as a function of the network density to describe the functional organization of the brain network. For each metric and for each density, we compared seizure-free versus late seizure-affected subjects using a Wilcoxon rank-sum statistic test. Density threshold study ensures that the networks of the two clinical groups have the same number of edges and that the between-group differences reflect alterations in brain organization rather than differences in level correlations. According to the recommendations reported in Hallquist and Hillary (2018), van den Heuvel et al. (2017), we assessed the extent to which the proportional thresholding includes spurious links in the brain networks by performing a permutation test to compare the distribution of the real FC values with the distribution of randomly generated FC values and find the maximum densities under which we have no spurious links (Nichols and Holmes, 2002; Muschelli et al., 2014). A detailed description of this test is reported in the Supplementary Material. Network density was defined as the number of the present connections divided by the number of all possible connections. We applied a wide range of density (D) ranging from 2% to 72% (maximum possible density after negative correlation removal) with increments by 2% and repeated the analysis for each density to find the best trade-off

Table 2

Recommended EpiBioS4Rx MRI Protocol to acquire resting state blood oxygen level dependent imaging (rs-BOLD), 3D T1-weighted magnetization prepared rapid gradient-echo (MPRAGE), and 3D T2-weighted fluid attenuated inversion recovery (FLAIR) sequences with 1.5 and 3T scanners. TE stands for echo time, TR for repetition time, TI inversion time, FOV for field of view and NEX for number of excitations.

Sequence	3D T1	RS-BOLD	3D T2 FLAIR
Plane	Sagittal or Axial	Oblique-Axial	Sagittal or Axial
Mode	3D	2D	3D
TR [ms]	1500–2500	2000	>5000
TE [ms]	Min	25	(Effective TE) 80–140
TI [ms]	1100–1500	n/a	2000–2500
Flip Angle	8–15°	78°	90°$\geqslant$120°
Frequency	256	64	256
Phase	256	64	256
NEX	$\geqslant$1	1	$\geqslant$1
FOV	256 mm	220 mm	256 mm
Slice Thickness	1 mm	3.4 mm	1 mm
Gap/Spacing	0	0.25	0
Parallel Imaging	Up to 2x	Up to 2x	Up to 2x

---

[2] http://www.nitrc.org/projects/conn.

Fig. 1. Flowchart of rs-fMRI and sMRI preprocessing. Top row outlines rs-fMRI preprocessing including realignment, centering, slice timing, outlier detection, normalization to the MNI 152 template, segmentation into cerebrospinal fluid (CSF), gray matter (GM) and white matter (WM), and smoothing. Bottom row shows the steps of sMRI preprocessing (centering, normalization to the MNI 152 template, segmentation into WM, GM and CSF) and the result of the denoising. Denoising includes linear regression of potential confounding effects: noise from WM, CSF subject motion and poor quality scans (outliers). After denoising, functional connectivity values between randomly-selected pairs of points (bottom right corner) show approximately centered distributions, with considerably reduced inter-subject variability.

between minimizing the number of spurious edges in each network and having a connected network with the inclusion of all the nodes. It is possible to see the effects of both weight-based and density-based thresholding on the overall connectivity in the Fig. S4.

For each network density, we computed the following network measurements at the whole-brain level: Network strength (S) concerning the intensity of the node connections and computed as the mean of all node strengths s_i:

$$s_i = \sum_j w_{ij};$$
(1)

where w_{ij} is weight associated to the edge between nodes i and j. global efficiency (G) and average shortest path length (L) to analyze graph integration that reflect the capacity of the network to transfer information and communicate between nodes.

Average shortest path length of the two mean networks was defined as the mean of the average shortest path lengths of all network nodes. By considering the distance between two nodes i and j the reciprocal of the edge weight $1/w_{ij}$, the average shortest path length of a node i is l_i^w

$$l_i^w = \frac{1}{N(N-1)} \sum_{i \neq j} d_{ij};$$
(2)

where N is the number of nodes in the network and d_{ij} is the shortest distance between two nodes.

Network global efficiency was computed as mean of the global efficiencies of network nodes. The length of an edge was designated as the reciprocal of the edge weight, therefore a high correlation coefficient can be interpreted as a short functional distance.

$$e_i^w = \frac{1}{N(N-1)} \sum_{i \neq j} \frac{1}{d_{ij}};$$
(3)

Clustering coefficient that indicates the degree to which nodes tend to cluster together and perform specialized processes. Clustering coefficient of the two mean networks was obtained by averaging the clustering coefficients c_i^w of all network nodes computed using the generalizations of clustering coefficient to weighted graphs according to Barrat definitions (Barrat et al., 2004).

$$c_i^w = \frac{1}{s_i(k_i - 1)} \sum_{j,h} \frac{w_{ij} + w_{ih}}{2} a_{ij} a_{ih} a_{jh};$$
(4)

s_i is the strength of node i, a_{ij} are elements of the adjacency matrix that indicates whether or not an edge exists, k_i is the node degree (number of edges connected to a node i), w_{ij} are the weights. The main idea of this generalization is to replace the total number of the triangles in which a node i participates, with the "intensity" of the triangle (Ma et al., 2018; La Rocca et al., 2018; Clemente and Grassi, 2018).

Characteristic clustering coefficient, characteristic average shortest path length and small-worldness were computed to compare the functional brain networks of the two clinical groups with a random network (Brier et al., 2014).

Many studies carried out across different modalities and scales have demonstrated that brain networks exhibit a small-world topology that allows the brain to optimize brain organization in term of integration and segregation. A graph is small-world if the path length is similar to that of a random graph $L/L^0 \sim 1$ and has a clustering coefficient that is much greater than a random graph $C/C^0 \gg 1$ where L^0 and C^0 are the mean clustering coefficient and the mean average shortest path length computed across 1000 Erdos Renyi random networks (Erdös and Rényi, 1959) generated in order to have the same number of nodes, edges, and degree distribution as the real network considered. Since, by definition, the study of the network topology comprises the analysis of network properties disregarding the weights, for each density, we studied small-

world behavior of the networks after binarizing them. Finally, we performed network hub analysis which is of paramount importance to study the critical ROI in the two TBI groups. Since hubs are nodes with a number of links that greatly exceeds, the average betweenness b_i of a node i was used to determine candidate hubs in a network. The betweenness was normalized as $B_i = b_i/B$ with B averaged betweenness for all nodes of the entire network. Then, we considered hubs all those nodes that are outliers of the normalized betweenness distribution of the network. Therefore, for each subject, we collected nodes having a betweenness greater than $Q_3 + 1.5*IQR$ where Q3 and IQR are the third quartile and the interquartile range of the betweenness distribution values, respectively (van den Heuvel and Sporns, 2013).

3. Results

3.1. Weighted metric analysis

Weighted average shortest path length and weighted global efficiency, computed to examine the integration properties for the mean networks of the seizure-free subjects and late seizure-affected subjects, are represented, for each network density, in Fig. 2. We underlined with red stars the densities to which a given network metric is significantly different ($p < 0.01$) for the two groups. Similarly, strength and weighted clustering coefficient, used to describe functional connectivity intensity and segregation of the mean brain networks relative to the two clinical groups, are reported for each density in Fig. 2. The seizure-affected group has, on average, a lower average shortest path length and clustering coefficinet, and a greater strength and global efficiency.

3.2. Topology analysis

It is well-known that healthy brain networks have a small-world topology. We investigated if TBI subjects maintain a small-world organization and whether seizure development affects brain network topology of the TBI cohort. We found that small-world index for the binary mean networks of seizure-free and late seizure-affected are, respectively 1.53 and 1.42. Both values are greater than 1 proving the small-worldness of the two group networks. However, examining characteristic clustering coefficient and characteristic average shortest path length, reported in Fig. 3 for the two groups, as a function of the network density, it is possible to notice that late seizure-affected subjects in the density interval highlighted by the red stars have significantly lower characteristic clustering coefficient and lower characteristic average shortest path length compared with seizure-free subjects. This suggests that late seizure-affected subjects tends to have a topology more similar to a random network resulting in a less efficient brain organization.

In seizure-free networks, all nodes are connected without network fragmentation for densities greater than 16 and in late seizure-affected networks, for densities greater than 24. It is interesting to notice that the density to which most of the computed metrics are significantly different for the seizure-free versus late seizure-affected comparison is 34. Therefore, we have chosen this density as the optimal density that guarantees to have all network nodes connected and at the same time significant differences between the two groups for all the graph metrics. Furthermore, from the results of the permutation test reported in the Supplementary Material (see Fig. S5), we found that the maximum densities under which we have no spurious links for the seizure-free group and for the seizure affected group are 59% and 56%,
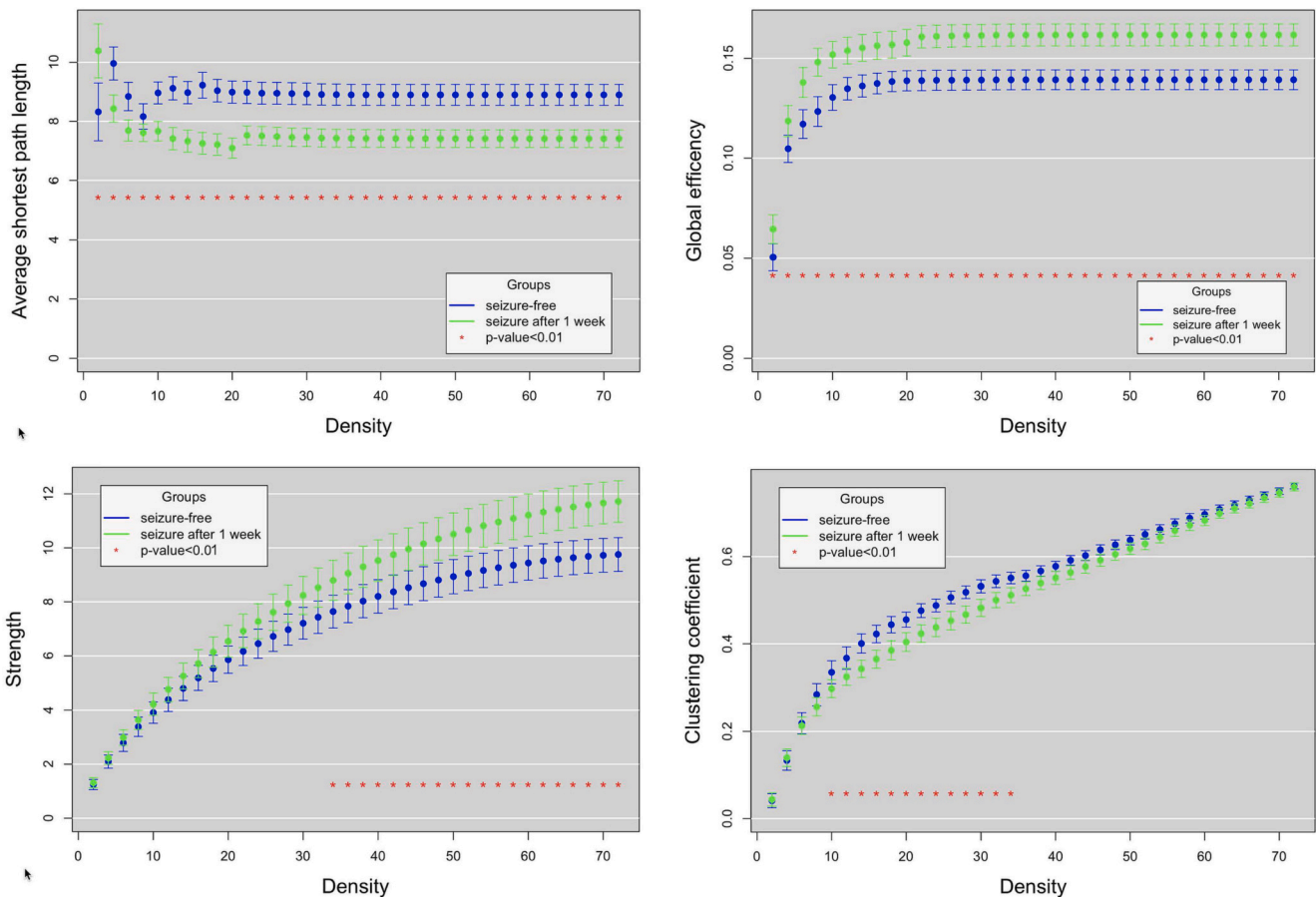

Fig. 2. Top row: Weighted average shortest path length (left) and weighted global efficiency (right) as a function of network density for seizure-free TBI patients (blue) and TBI patients who de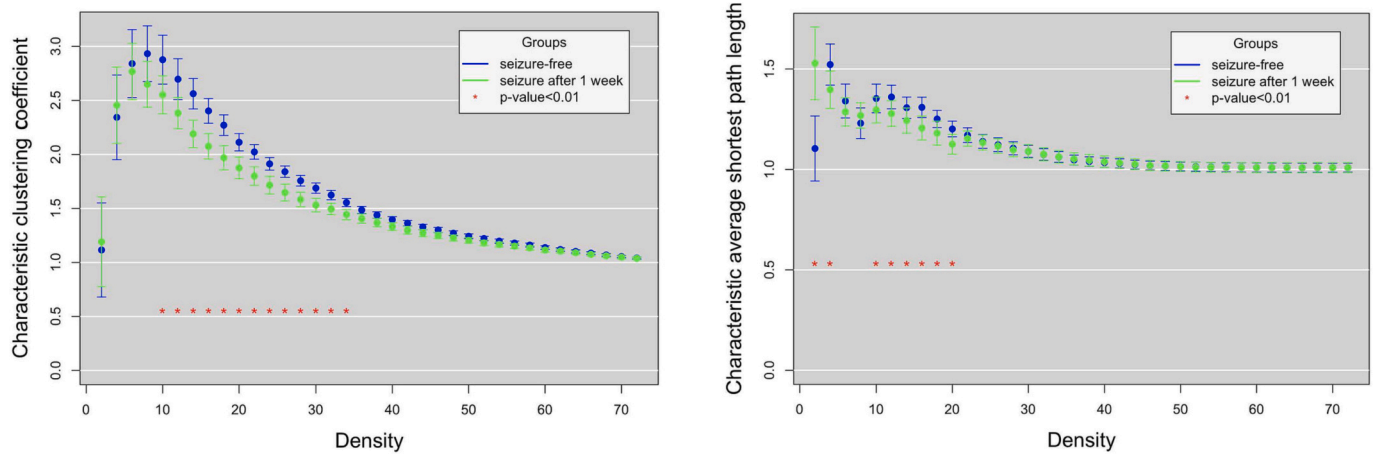veloped seizure at least one week post-injury (green). Bottom row: Strength (left) and weighted clustering coefficient (right) as a function of network density for seizure-free TBI patients (blue) and TBI patients who developed seizure at least one week post-injury (green).

Fig. 3. Characteristic clustering coefficient (left) and characteristic average shortest path length (right) as a function of network density for seizure-free TBI patients (blue) and TBI patients who developed seizure at least one week post-injury (green).

respectively. These densities are greater than the optimal thresholds that we found experimentally, therefore our analysis is not affected by spurious link. Table 3 shows the network metric values and the statistical significance obtained from the comparison of the two groups at the optimal density of 34. According to the recommendation in van den Heuvel et al. (2017), we also controlled for differences in overall FC values between the two groups and we found that both before and after the thresholding there are no significant differences (see Fig. S6 in the Supplementary Material).

3.3. Hub detection

We used the optimal density threshold of 34 to carry out the hub detection and analysis for the two group comparison. Fig. 4 shows in red the hubs for the late seizure-affected group and in cyan the hubs for the

Table 3

Values and statistical significance of the network metrics (strength, weighted average shortest path length, weighted global efficiency, weighted clustering coefficient, characteristic clustering coefficient, characteristic average shortest path length) obtained from the comparison between seizure-free subjects and late seizure-affected subjects at a network density of 34%, the optimal threshold at which all the network metrics (except for the characteristic average shortest path length) are significantly different and all the ROIs are included in the network. The table reports also the 95 percent confidence interval (CI) for the difference between population medians and the effect size for non-parametric test computed as $\frac{Z}{\sqrt{N}}$ where Z stands for Z statistic and N is the number of observables.
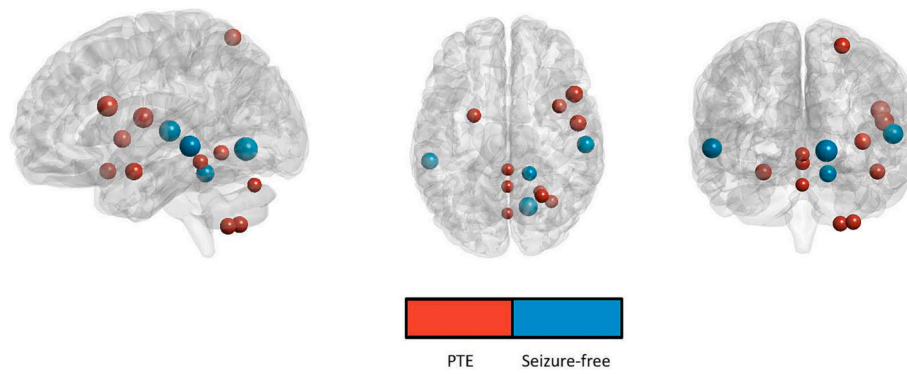
Metric	Seizure-free	Late seizure-affected	p-value	CI	Effect size
Strength	7.64 ± 0.61	8.80 ± 0.74	$8.89 \cdot 10^{-3}$	[0.93, 2.47]	0.59
Average shortest path length	8.91 ± 0.36	7.43 ± 0.30	$2.20 \cdot 10^{-16}$	[−2.51, −1.19]	0.87
Global efficiency	0.14 ± 0.01	0.16 ± 0.01	$6.70 \cdot 10^{-12}$	[0.02, 0.04]	0.71
Clustering coefficient	0.55 ± 0.01	0.51 ± 0.02	$1.51 \cdot 10^{-3}$	[−0.05, −0.03]	0.87
Characteristic clustering coefficient	1.55 ± 0.04	1.44 ± 0.05	$1.51 \cdot 10^{-3}$	[−2.34, −0.78]	0.67
Characteristic average shortest path length	1.06 ± 0.03	1.06 ± 0.03	> 0.01	–	–

seizure-free group. In the late seizure-affected group, the network hubs have, on average, a lower betweenness but are greater in number. Table 4 reports the betweenness values and the anatomical regions of the AAL atlas corresponding to the hubs of the two groups.

In addition, to investigate how brain lesions are related to the functional brain networks, we identified the anatomical regions of the AAL that are affected by lesions in the highest number of subjects for both clinical groups. Figs. 5 and 6 show the original positive connectivity matrix, the connectivity matrix at the threshold chosen as optimal and the connections between the regions affected by lesions (in the highest number of subjects) for the seizure-affected group and the seizure-free group, respectively. These results suggest that lesions are responsible for a reduction in brain connectivity and this is particularly evident in the late seizure-affected group. An exhaustive list of the AAL regions mainly affected by lesions for the two groups is reported in the Supplementary Material (Table S1).

4. Discussion

In this study, we utilized graph theory to investigate the functional connectivity of seizure-free TBI patients and late seizure-affected TBI patients. We found that patients who have developed seizures more than 1 week after a TBI exhibited an overall increase in functional connectivity in their brain networks. Indeed, strength is significantly greater in seizure-affected subjects than in seizure-free subjects along a wide range of densities (34–72%). Increased connectivity could explain why increased weighted global efficiency was observed in TBI patients who develop epilepsy. Nevertheless, weighted global efficiency, by definition, does not depend only on network weights but also on routing paths. Therefore, the significant enhanced in global efficiency and the significant reduction in weighted average shortest path length along all density range (2–72%) could also suggest an intrinsic alteration in brain wiring patterns that implies a hyperactive functional integration and a faster transmission between different brain regions. In addition to increased weighted global efficiency, participants with seizures occurring more than 1 week after injury had decreased weighted clustering coefficient compared with the seizure-free patients, which may be explained by an impaired functional segregation of late seizure-affected TBI patients. Thus, the resultant hyperconnectivity and hyperintegration within functional networks, and at the same time the lack of an efficient local connectedness and segregation may reflect the pathological mechanism of the functional networks responsible for seizure propagation and rapid uncontrolled information flow from the seizure onset zone. However, functional hyperconnectivity is a common phenomenon in brain disorders, and is thought to be due to the plasticity and compensatory

Fig. 4. Glass brain with the network hubs for the late seizure-affected group in red and the seizure-free group in cyan. From the left to the right the sagittal, axial and coronal views of the glass brain are shown for late seizure-affected vs. seizure-free subjects. The size of each hub is proportional to the corresponding node betweenness.

Table 4
Betweenness values and anatomical regions of the AAL atlas corresponding to the hubs of the two groups: seizure-free and late seizure-affected subjects. In the table R stands for right, L for left, Sup for superior, Inf for inferior and Mid for Middle.

Group	Region	Hub betweenness
Seizure-free	R Lingual Gyrus	5.04
Seizure-free	R Sup Temporal Gyrus	4.45
Seizure-free	L Mid Temporal Gyrus	4.32
Seizure-free	R Cerebelum 4 5	3.46
Seizure-affected	R Inf Frontal Operculum	4.27
Seizure-affected	R Rolandic Operculum	4.14
Seizure-affected	R Insula	3.30
Seizure-affected	L Amygdala	3.27
Seizure-affected	R Sup Parietal Gyrus	3.11
Seizure-affected	R Sup Temporal Pole	3.05
Seizure-affected	R Cerebelum 7b	2.93
Seizure-affected	R Cerebelum 8	2.89
Seizure-affected	Vermis 3	2.60
Seizure-affected	Vermis 4 5	2.60
Seizure-affected	Vermis 7	2.34

mechanisms of the human brain but specific biological mechanisms are not conclusive. Therefore another possible explanation is that the brains of TBI patients with epilepsy require a greater continuous selection of alternative paths to maintain normal function by adaptively reorganizing regional connectivity profiles in response to TBI-induced damage (Mazrooyisebdani et al., 2020; Hillary et al., 2015).

In this work, we also binarized the functional networks of TBI patients to study their brain network topology and how this changes in association with seizure development. Although whole-brain functional networks of late seizure-affected subjects showed small-world properties like that of seizure-free subjects, characteristic clustering coefficient, reflecting the degree of closeness between neighboring brain regions compared with a random network, was lower in late seizure-affected subjects than in seizure-free network. In terms of characteristic average shortest path length, there is no apparent difference between seizure-free and late seizure-affected TBI patients at most density levels. Late seizure-affected, however, showed a lower characteristics average shortest path length at a few densities (4% and 10–20%). Nevertheless, the significant differences in average characteristic shortest path length occur at densities for which some nodes are isolated, and this might introduce a bias in the interpretation of the results for those densities. The characteristic clustering coefficient and average shortest path length trends suggest a greater tendency toward random network configuration of functional brain networks in TBI patients with epilepsy. Whereas seizure-free TBI subjects demonstrate to have a better balance between integration and segregation.

Concerning the network hubs, we identified 11 nodes with a large number of connections in the late seizure-affected group, and 4 nodes in the seizure-free group. The higher number of hubs in the seizure-affected group is in line with the hyperconnectivity shown with the graph-theory metrics, but also with a compensatory mechanism that tends to form more lower betweenness hubs to replace the higher betweenness hubs compromised by the trauma that tends to reduce functional connectivity. Interestingly, in the seizure-affected group 6/11 hubs were located in limbic structures (including amygdala, insula, and part of the opercula of the insula) and the temporal lobe, and 5/11 nodes were located in the cerebellum. Previous studies have shown that
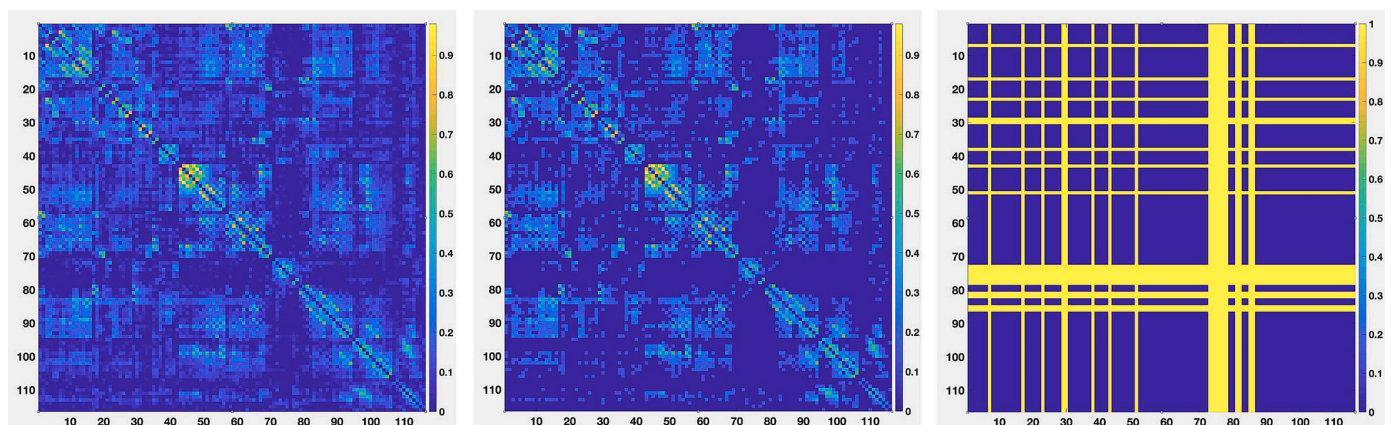
Fig. 5. This figure shows, for the seizure-affected subjects, the original positive connectivity matrix (left), the connectivity matrix at the optimal density of 34 (center) and connections between AAL regions that are affected by lesions in the highest number of seizure-affected subjects (right).
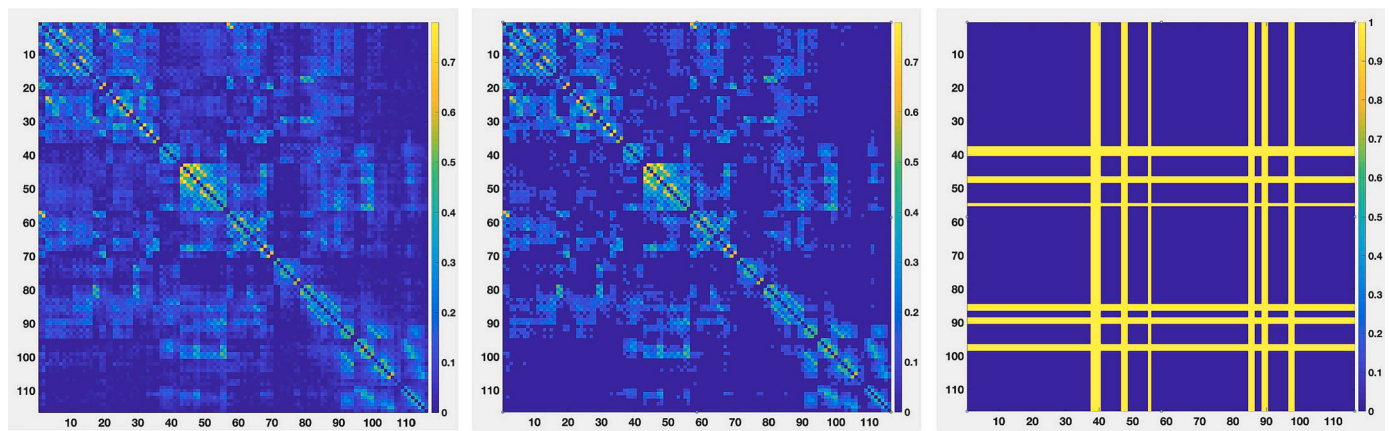
Fig. 6. This figure shows, for the seizure-free subjects, the original positive connectivity matrix (left), the connectivity matrix at the optimal density of 34 (center) and connections between AAL regions that are interested by lesions in the highest number of seizure-free subjects (right).

patients with epilepsy present functional hyperconnectivity in the temporal lobe, limbic system, and the cerebellum (Haneef et al., 2014; Zhong et al., 2011). For example, the insular cortex, a structure involved in diverse functions such as motor control, somatosensory processing, cognition and emotional experience, is affected in patients with temporal lobe epilepsy, evidenced by histological and volumetric changes (Sudbury and Avoli, 2007); is involved in the epileptic manifestations and seizure propagation (Isnard et al., 2000); and is activated during generalized seizures (Gotman et al., 2005). Similarly, increased connectivity, perfusion, and atrophy in the cerebellum of patients with Focal and Generalized Epilepsy has also been reported in previous studies (Haneef et al., 2014; Zhong et al., 2011; Gotman et al., 2005; Norden and Blumenfeld, 2002). The cerebellum contains somatotopic representations of the face and limbs, with potential implications in the the motor manifestations of an epileptic seizures (Norden and Blumenfeld, 2002). Moreover, previous experimental models have demonstrated a significant involvement of the cerebellum during spike-and-wave discharges, independently of rhythmic movement, suggesting that cerebellar neurons may play a critical role in the development and maintenance of the spike-and-wave rhythmicity and seizures (Kandel and Buzsáki, 1993).

Our results are consistent with many previous studies reporting altered functional connectivity and structural connectivity in subjects with epilepsy (Jiang et al., 2017), even though a direct comparison is not possible for two main factors: (i) This is the first study that examines functional connectivity in patients with seizures occurring after a TBI using graph theory; (ii) Prior literature has performed functional brain network studies comparing subjects with epilepsy and normal controls, in the proposed work we analyze a cohort of only TBI patients who have or have not developed late seizures. Even though graph theory applied to the study of functional connectivity in TBI patients are proved to be a promising and powerful instrument to detect alterations connected to seizure development, further investigations are necessary to obtain conclusive results on the integration and segregation of TBI patients' functional networks. Moving graph metrics into the clinic should be still approached with caution, indeed TBI heterogeneity and the fact that fMRI acquisition protocols and brain network construction and analysis vary substantially across studies make study reproducibility very challenging. We hope that this work could help to carry on the research in this direction in order to understand which graph metrics can be used as clinical biomarkers. In upcoming years, EpiBioS4Rx will enroll up to 300 patients and will conduct longitudinal follow-ups for two years to assess seizure outcomes. Therefore, we will be able to validate these results on a larger and more reliable dataset. In the future, with a larger dataset, we plan also to investigate the debated topic of the negative functional correlation coefficients and we plan to use machine learning techniques

to assess the sensitivity and specificity of the proposed graph metrics in detecting PTE patients.

5. Conclusions

In this work, we used graph theory to examine functional connectivity in TBI patients who have and have not developed late seizures. Our results show that the late seizure-affected group has functional networks that are hyperconnected, hyperintegraed but at the same time hyposegregated compared with seizure-free patients. This may reflect the rapid but uncontrolled 'flow of information' responsible for seizure onset and propagation. In addition, seizure-affected group show a more compromised balance between integration and segregation and a greater number of hubs that however have a less strategical role in terms of connections that crosses them.

Author contribution

M.L.R. and D.D. conceived the work. M.L.R., R.G. and S.R conducted the data processing. M.L.R. conducted the analyses and wrote the manuscript. G.B. and P.V. reviewed clinically the work. All authors M.L.R., G.B., R.G., S.R., N.A., M.M., P.V., R.B., D.E, A.T. and D.D. analyzed the results, reviewed the manuscript, approved the final version to be published and agreed to be accountable for the integrity and accuracy of all aspects of the work.

Ethical publication statement

We confirm that we have read the Journal's position on issues involved in ethical publication and affirm that this report is consistent with those guidelines. This work was approved by the UCLA Institutional Review Board (IRB # 16–001 576) and the local review boards at each EpiBioS4Rx Study Group institution. Assent and written consent was obtained from the legal representative as per state law. All patients have consented for data to be deidentified and then analyzed.

Data statement

The data analyzed in this study is subject to the following licenses/

restrictions: access to data must be requested and approved by the EpiBioS4Rx steering committee. Requests to access these datasets should be directed to epibiossteeringcommittee@loni.usc.edu.

Appendix A. Supplementary data

Supplementary data associated with this article can be found, in the online version, at https://doi.org/10.1016/j.nbd.2023.106053.

References

Achard, S., Bullmore, E., 2007. Efficiency and cost of economical brain functional networks. PLoS Comput. Biol. 3 (2), e17.

Ashburner, J., 2009. Computational anatomy with the spm software. Magn. Reson. Imaging 27 (8), 1163–1174.

Barrat, A., Barthelemy, M., Pastor-Satorras, R., Vespignani, A., 2004. The architecture of complex weighted networks. Proc. Nat. Acad. Sci. 101 (11), 3747–3752.

Bellantuono, L., Marzano, L., La Rocca, M., Duncan, D., Lombardi, A., Maggipinto, T., Monaco, A., Tangaro, S., Amoroso, N., Bellotti, R., 2021. Predicting brain age with complex networks: From adolescence to adulthood. NeuroImage 225, 117458.

Brier, M.R., Thomas, J.B., Fagan, A.M., Hassenstab, J., Holtzman, D.M., Benzinger, T.L., Morris, J.C., Ances, B.M., 2014. Functional connectivity and graph theory in preclinical alzheimer's disease. Neurobiol. Aging 35 (4), 757–768.

Cavazos, J., Verellen, R., 2010. Post-traumatic epilepsy: an overview. Therapy 7 (5), 527.

Clemente, G.P., Grassi, R., 2018. Directed clustering in weighted networks: A new perspective. Chaos Soliton. Fract. 107, 26–38.

Erdös, P., Rényi, A., 1959. On random graphs i. Publ. Math. Debrecen 6, 290.

Fox, M.D., Snyder, A.Z., Vincent, J.L., Corbetta, M., Van Essen, D.C., Raichle, M.E., 2005. The human brain is intrinsically organized into dynamic, anticorrelated functional networks. Proc. Nat. Acad. Sci. 102 (27), 9673–9678.

Garner, R., La Rocca, M., Vespa, P., Jones, N., Monti, M.M., Toga, A.W., Duncan, D., 2019. Imaging biomarkers of posttraumatic epileptogenesis. Epilepsia 60 (11), 2151–2162.

Geerligs, L., Henson, R.N., et al., 2016. Functional connectivity and structural covariance between regions of interest can be measured more accurately using multivariate distance correlation. NeuroImage 135, 16–31.

Gotman, J., Grova, C., Bagshaw, A., Kobayashi, E., Aghakhani, Y., Dubeau, F., 2005. Generalized epileptic discharges show thalamocortical activation and suspension of the default state of the brain. Proc. Nat. Acad. Sci. 102 (42), 15236–15240.

Hallquist, M.N., Hillary, F.G., 2018. Graph theory approaches to functional network organization in brain disorders: A critique for a brave new small-world. Netw. Neurosci. 3 (1), 1–26.

Haneef, Z., Lenartowicz, A., Yeh, H.J., Levin, H.S., Engel Jr., J., Stern, J.M., 2014. Functional connectivity of hippocampal networks in temporal lobe epilepsy. Epilepsia 55 (1), 137–145.

Hillary, F.G., Roman, C.A., Venkatesan, U., Rajtmajer, S.M., Bajo, R., Castellanos, N.D., 2015. Hyperconnectivity is a fundamental response to neurological disruption. Neuropsychology 29 (1), 59.

Isnard, J., Guénot, M., Ostrowsky, K., Sindou, M., Mauguière, F., 2000. The role of the insular cortex in temporal lobe epilepsy. Ann. Neurol.: Offic. J. Am. Neurol. Assoc. Child Neurol. Soc. 48 (4), 614–623.

Jenkinson, M., Beckmann, C.F., Behrens, T.E., Woolrich, M.W., Smith, S.M., 2012. Fsl. Neuroimage 62 (2), 782–790.

Jiang, W., Li, J., Chen, X., Ye, W., Zheng, J., 2017. Disrupted structural and functional networks and their correlation with alertness in right temporal lobe epilepsy: A graph theory study. Front. Neurol. 8, 179.

Kandel, A., Buzsáki, G., 1993. Cerebellar neuronal activity correlates with spike and wave eeg patterns in the rat. Epilepsy Res. 16 (1), 1–9.

La Rocca, M., Amoroso, N., Monaco, A., Bellotti, R., Tangaro, S., Initiative, A.D.N., et al., 2018. A novel approach to brain connectivity reveals early structural changes in alzheimer's disease. Physiol. Meas. 39 (7), 074005.

La Rocca, M., Barisano, G., Bennett, A., Garner, R., Engel, J., Gilmore, E.J., McArthur, D. L., Rosenthal, E., Stanis, J., Vespa, P., et al., 2021. Distribution and volume analysis of early hemorrhagic contusions by mri after traumatic brain injury: a preliminary report of the epilepsy bioinformatics study for antiepileptogenic therapy (epibios4rx). Brain Imaging Behav. 15 (6), 2804–2812.

La Rocca, M., Garner, R., Amoroso, N., Lutkenhoff, E.S., Monti, M.M., Vespa, P., Toga, A. W., Duncan, D., 2020. Multiplex networks to characterize seizure development in traumatic brain injury patients. Front. Neurosci. 14, 1238.

Liao, W., Zhang, Z., Pan, Z., Mantini, D., Ding, J., Duan, X., Luo, C., Lu, G., Chen, H., 2010. Altered functional connectivity and small-world in mesial temporal lobe epilepsy. PloS One 5 (1).

Lucke-Wold, B.P., Nguyen, L., Turner, R.C., Logsdon, A.F., Chen, Y.-W., Smith, K.E., Huber, J.D., Matsumoto, R., Rosen, C.L., Tucker, E.S., et al., 2015. Traumatic brain injury and epilepsy: underlying mechanisms leading to seizure. Seizure 33, 13–23.

Ma, X., Jiang, G., Fu, S., Fang, J., Wu, Y., Liu, M., Xu, G., Wang, T., 2018. Enhanced network efficiency of functional brain networks in primary insomnia patients. Front. Psychiatry 9, 46.

Mazrooyisebdani, M., Nair, V.A., Garcia-Ramos, C., Mohanty, R., Meyerand, E., Hermann, B., Prabhakaran, V., Ahmed, R., 2020. Graph theory analysis of functional connectivity combined with machine learning approaches demonstrates widespread

network differences and predicts clinical variables in temporal lobe epilepsy. Brain Connect. 10 (1), 39–50.

Muschelli, J., Nebel, M.B., Caffo, B.S., Barber, A.D., Pekar, J.J., Mostofsky, S.H., 2014. Reduction of motion-related artifacts in resting state fmri using acompcor. Neuroimage 96, 22–35.

Nichols, T.E., Holmes, A.P., 2002. Nonparametric permutation tests for functional neuroimaging: a primer with examples. Hum. Brain Mapp. 15 (1), 1–25.

Norden, A.D., Blumenfeld, H., 2002. The role of subcortical structures in human epilepsy. Epilepsy Behav. 3 (3), 219–231.

Pandit, A.S., Expert, P., Lambiotte, R., Bonnelle, V., Leech, R., Turkheimer, F.E., Sharp, D.J., 2013. Traumatic brain injury impairs small-world topology. Neurology 80 (20), 1826–1833.

Peterson, A.B., Xu, L., Daugherty, J., Breiding, M.J., 2019. Surveillance report of traumatic brain injury-related emergency department visits, hospitalizations, and deaths, united states, 2014. CDC.

Rasero, J., Amoroso, N., La Rocca, M., Tangaro, S., Bellotti, R., Stramaglia, S., Initiative, A.D.N., 2017. Multivariate regression analysis of structural mri connectivity matrices in alzheimer's disease. PLoS One 12 (11), e0187281.

Rubinov, M., Sporns, O., 2010. Complex network measures of brain connectivity: uses and interpretations. Neuroimage 52 (3), 1059–1069.

Schwarz, A.J., McGonigle, J., 2011. Negative edges and soft thresholding in complex network analysis of resting state functional connectivity data. Neuroimage 55 (3), 1132–1146.

Sharma, S., Tiarks, G., Haight, J., Bassuk, A.G., 2021. Neuropathophysiological mechanisms and treatment strategies for post-traumatic epilepsy. Front. Mol. Neurosci. 14, 612073.

Smitha, K., Akhil Raja, K., Arun, K., Rajesh, P., Thomas, B., Kapilamoorthy, T., Kesavadas, C., 2017. Resting state fmri: A review on methods in resting state connectivity analysis and resting state networks. Neuroradiol. J. 30 (4), 305–317.

Song, J., Nair, V.A., Gaggl, W., Prabhakaran, V., 2015. Disrupted brain functional organization in epilepsy revealed by graph theory analysis. Brain Connect. 5 (5), 276–283.

Sudbury, J.R., Avoli, M., 2007. Epileptiform synchronization in the rat insular and perirhinal cortices in vitro. Eur. J. Neurosci. 26 (12), 3571–3582.

Tijms, B.M., Wink, A.M., de Haan, W., van der Flier, W.M., Stam, C.J., Scheltens, P., Barkhof, F., 2013. Alzheimer's disease: connecting findings from graph theoretical studies of brain networks. Neurobiol. Aging 34 (8), 2023–2036.

Tzourio-Mazoyer, N., Landeau, B., Papathanassiou, D., Crivello, F., Etard, O., Delcroix, N., Mazoyer, B., Joliot, M., 2002. Automated anatomical labeling of activations in spm using a macroscopic anatomical parcellation of the mni mri single-subject brain. Neuroimage 15 (1), 273–289.

van den Heuvel, M.P., de Lange, S.C., Zalesky, A., Seguin, C., Yeo, B.T., Schmidt, R., 2017. Proportional thresholding in resting-state fmri functional connectivity networks and consequences for patient-control connectome studies: Issues and recommendations. Neuroimage 152, 437–449.

van den Heuvel, M.P., Sporns, O., 2013. Network hubs in the human brain. Trends Cogn. Sci. 17 (12), 683–696.

Vlooswijk, M., Vaessen, M., Jansen, J., de Krom, M., Majoie, H., Hofman, P., Aldenkamp, A., Backes, W., 2011. Loss of network efficiency associated with cognitive decline in chronic epilepsy. Neurology 77 (10), 938–944.

Wang, J., Qiu, S., Xu, Y., Liu, Z., Wen, X., Hu, X., Zhang, R., Li, M., Wang, W., Huang, R., 2014. Graph theoretical analysis reveals disrupted topological properties of whole brain functional networks in temporal lobe epilepsy. Clin. Neurophysiol. 125 (9), 1744–1756.

Wang, J., Zuo, X., He, Y., 2010. Graph-based network analysis of resting-state functional mri. Front. Syst. Neurosci. 4, 16.

Wang, Z., Jie, B., Bian, W., Zhang, D., Shen, D., Liu, M., 2019. Adaptive thresholding of functional connectivity networks for fmri-based brain disease analysis. In: International Workshop on Graph Learning in Medical Imaging. Springer, pp. 18–26.

Watts, D.J., Strogatz, S.H., 1998. Collective dynamics of 'small-world' networks. Nature 393 (6684), 440.

Whitfield-Gabrieli, S., Nieto-Castanon, A., 2012. Conn: a functional connectivity toolbox for correlated and anticorrelated brain networks. Brain Connect. 2 (3), 125–141.

Yang, H., Ren, J., Wang, Q., 2018. Abnormal brain network in epilepsy and associated comorbidites. Neuropsychiatry (London).

Yushkevich, P.A., Piven, J., Hazlett, H.C., Smith, R.G., Ho, S., Gee, J.C., Gerig, G., 2006. User-guided 3d active contour segmentation of anatomical structures: significantly improved efficiency and reliability. Neuroimage 31 (3), 1116–1128.

Zhong, Y., Lu, G., Zhang, Z., Jiao, Q., Li, K., Liu, Y., 2011. Altered regional synchronization in epileptic patients with generalized tonic–clonic seizures. Epilepsy Res. 97 (1–2), 83–91.